LA-UR -84-729

CONF-8310229--8

Los Alamos National Laboratory is operated by the University of California for the United States Department of Energy under contract W-7405-ENG-36.

LA-UR--84-729

DE84 007480

TITLE: Three-Dimensional Computer Modeling of Dynamic Reconnection in the Magnetotail

AUTHOR(S): J. Birn

SUBMITTED TO: Chapman Conference Proceedings on Magnetic Reconnection, 3-7 October 1983, Los Alamos, NM

DISCLAIMER

MASTER

Los Alamos Los Alamos National Laboratory
Los Alamos, New Mexico 87545

FORM NO 836 R4
ST NO 2629 5/81

Three-Dimensional Computer Modeling of Dynamic Reconnection in the Magnetotail

Joachim Birn

Los Alamos National Laboratory

Los Alamos, NM 87545

Abstract

Two- and three-dimensional computer models of the dynamics of the magnetosphere and in particular the magnetotail have shown, that the basic features of the idealized linear or steady state reconnection theory are still found in time dependent and spatially more complicated configurations such as the magnetotail, which basically resembles a plane sheet pinch but in addition has small magnetic field components perpendicular to the sheet, field line flaring and variations along both directions parallel to the current sheet. These basic features are the formation of a magnetic neutral X-line or separator, where two surfaces separating magnetic fluxes of different topology intersect, with the generation of an electric field along the separator and the production of strong plasma flows parallel to the current sheet away from the separator in opposite directions.

In addition, the computer models of magnetotail dynamics have produced many large scale features that are directly observed or deduced from observation in relation with magnetospheric substorms. Among those features are: the thinning of the plasma sheet, the formation of a plasmoid, a region of closed magnetic loops detached from Earth, which moves tailward at a speed of several hundreds of km/sec, and the generation of field-aligned currents.

In view of the recent discovery of plasmoid signatures in the distant magnetotail at about 200 R_E from ISEE-3 satellite measurements, we discuss the properties of the plasmoid in the computer simulations, in particular its topology, spatial extent and speed, the current system associated with it and its local appearance at a fixed location in space. Furthermore, we discuss the conversion of the energy flux around the separator, current deviations and the occurrence of field-aligned currents and their generation by shear flows.

1. Introduction

MHD computer models have been used with great success to model reconnection in the earth's magnetosphere and magnetotail. They have been able to show that indeed reconnection can be a very powerful converter of magnetic energy into kinetic energy by a topological change of the magnetic field configuration connected with the formation of magnetic neutral lines. The typical flow pattern around the X-type neutral line or separator predicted by steady state models (Sweet, 1958; Parker, 1963; Petschek, 1964) was found for a variety of different initial and boundary conditions and resistivity models.

The major drawback of these large scale models so far is that the diffusion process that is necessary to enable reconnection was based on some more or less ad hoc model of anomalous resistivity. Whereas this probably has not much effect on the large scale spatial structures of the models, resistive MHD theory has its limitations when finer scales in space and time are considered. In particular, the time scale of the instabilities depends basically on the more or less arbitrary resistivity and the resistive MHD models cannot tell what actually happens within the so-called diffusion region, where deviations from the ideal Ohm's law $\underline{E} + \underline{v} \times \underline{B} = 0$ are important.

There are, however, still many features and structural details, not present in the simplified reconnection theories, that can be explained by a time-dependent MHD model using more realistic two- and three-dimensional geometries. In this paper we will discuss those features on the basis of three-dimensional MHD simulations of reconnection in the magnetotail. In view of the discovery of plasmoid signatures in the distant tail (Hones et al., 1983) the emphasis will be on the properties of the plasmoid found in the computer simulations, its topology, spatial extent and speed, the current system associated with it and its local appearance at different fixed

locations. Furthermore, we will discuss current deviations in the reconnection region, the generation of field-aligned currents, and the energy flux in the reconnection region.

2. The model, initial and boundary conditions

The computer model uses an explicit leapfrog scheme to solve the non-linear time-dependent MHD equations including constant resistivity. (For more details, see Birn and Hones, 1981; Birn, 1976).

The initial configurations are self-consistent three-dimensional equilibrium models of the magnetotail (Birn, 1979) as shown in Figure 1. The figure shows a quarter cross-section of the tail with the earth somewhere to the left. Full lines with arrows indicate magnetic field lines and the hatched region indicates the plasma sheet. The width of the plasma sheet is defined here not by the transition from closed plasma sheet field lines to open lobe field lines but by the scaling distance on which, for instance, the plasma pressure drops by some factor 2 or 3. The model still basically resembles a plane one-dimensional sheet pinch. There are, however, small, but possibly important, deviations. The first one is the presence of a small normal magnetic field component in the z direction, which is positive in the neutral sheet and become negative in the lobes. This is connected with a flaring of the lobe field lines and a decrease of field strength with distance from the earth. The second one is the presence of a y component of the magnetic field which leads to a flaring also in the y direction adding to the decrease in field strength. The third one is a variation (here increase) of plasma sheet thickness and correspondingly the normal field B_z across the tail in the y direction toward dawn and dusk. This is optional and we will compare its effect by comparison with simulations starting from a configuration without such variation (but still presence of B_z and B_y and the corresponding flaring).

The actual computation system was a rectangular box (indicated by dashed lines). The size of the box was 10 units in the y and z directions and 64 units in the x direction, all expressed in terms of the typical scale length (plasma sheet half width) in the z direction. Assuming a scale length of 2 to 3 R_E the system is close to the actual size of the magnetotail with a length comparable to the distance recently explored by the ISEE 3 satellite. Symmetry was imposed at the boundary planes y=0 and z=0. At the other boundaries we kept the normal magnetic field fixed and set the velocity equal to 0. This is of course not realistic, it corresponds, however, to the boundary condition usually used for stability analysis and is probably the most stable one.

3. The time-dependent evolution

The time-dependent evolution of the system is initiated by the occurrence of (anomalous) resistivity which causes the system to diffuse slowly. Out of the perturbations grows the tearing-like instability on a faster time scale.

We will discuss the evolution and the influence of several parameters in the model on the basis of four different runs (see Table 1). These parameters are:

1) The increase of the plasma sheet thickness and the magnitude of B_z with $|y|$ expressed by the factor λ.
2) The lobe density n_L; in the numerical code, a finite lobe density, somewhat higher than real, has to be imposed in order to limit the wave propagation speed which determines the maximum possible time step; the value of n_L given in Table 1 is normalized by the difference between the maximum plasma sheet density and the lobe density. Since constant temperature is assumed, n_L also represents the lobe pressure normalized in the same way as the density.

3) The resistivity, which influences the time scale of the unstable growth and possibly also the wave length of the most unstable mode. The parameter S in Table 1 is the magnetic Reynolds number or Lindquist number which is equal to the inverse resistivity in normalized units.

As a reference case we use the evolution of the fields as published by Birn and Hones (1981), case A of Table 1, shown in figure 2 and 3. Figure 2 shows magnetic field lines in the midnight meridian plane (y=0) for different times (in units of a typical Alfven travel time of about 10-15 sec). We can see plasma sheet thinning, and the formation of closed magnetic loops, the plasmoid that subsequently moves tailward. The structures within the plasmoid may or may not be related to reflections at the far boundary which was assumed to be closed in this run. We will see later that there are characteristic features probably not caused by boundary effects.

The evolution of the velocity field is shown in Figure 3 in the equatorial plane z = 0 by arrows representing velocity vectors. The earth is again to the left. The maximum length of the vectors corresponds roughly to the typical Alfven speed of the order of 1000 km/sec. The dotted line indicates the neutral line, which consists of X-points in its earthward part and O-points in the tailward part of a closed line. We can see that reconnection and the occurrence of fast flow are restricted in the y direction to about half the width of the tail or less. To demonstrate the cause for this result we compare this figure with the corresponding figure resulting from run B without the plasma sheet thickening toward the flanks of the tail, shown in Figure 4 in the same kind of representation as in Figure 3. We see that now reconnection and fast flow extends across the whole tail even though we used the very restrictive boundary conditions $\underline{v}$=0 at the boundary in y.

The magnetic field evolution of this case is shown in Figure 5 again in the x,z plane. It looks very similar to the evolution of the reference case (Figure 2). Remarkable, however, is the more pronounced dent at the near earth end of the plasmoid. This is most likely not a result of reflections at the tailward boundary. A very similar result was obtained by Sato and Hayashi (1979) in a simulation of driven reconnection with open boundary conditions. The cause of this dent is a reversal of the current direction in this region which will be discussed later. Notice that a satellite crossing this region would see an apparent neutral sheet crossing.

Now let us study the effect of the enhanced lobe density. Figure 6 shows the magnetic field evolution for case C with reduced lobe density. It is again very similar to the previous figures. Figure 6, however, shows more clearly the characteristic wavelength in the x direction leading to a multiple island structure. This waviness was also present in the first example but could not be seen in the magnetic field figure. The wavelength is very close to the wavelength of the mode that is expected to grow fastest in the linear tearing theory of a one-dimensional current sheet for a magnetic Reynolds number S=200 as used for the simulations discussed so far. This wavelength should increase with increasing magnetic Reynolds number proportional to $S^{1/4}$. We have therefore performed another run with S=1000, run D of Table 1, also to see the effect on the temporal evolution. A part of the evolution is shown in Figure 7 in the same format as Figures 2, 5, and 6. The first thing to point out is the time scale of the figures shown at the right side. Because of the slower diffusion it takes much longer for the instability to grow from the "diffusion noise".

The next thing to look for is the wavelength of the structures in the x direction. It is similar to that in Figure 6, actually even a little bit shorter. This indicates that the wavelength of this characteristic wave is probably not the typical resistivity dependent wavelength of the fastest tearing mode as in usual linear tearing theory. It seems possible that these waves actually represent ideal MHD modes which produce multiple neutral lines only as a side effect when resistivity allows it. The fact that stable waves of similar periods of 5-10 minutes are a common feature in magnetotail observations support this view.

The third feature present in run D is the filamentation in the z direction which starts as a dent in the near earth end of the plasmoid and leads to the formation of multiple islands also in the z direction. It is difficult from single satellite observations in a configuration like this to identify "neutral sheet" crossings. It is very unlikely that these features are caused by boundary reflections because the plasma does not hit the right boundary before the time of the last frame.

Now, let us see what the magnetic field evolution would look like at some fixed locations within the system. Figure 8 shows the evolution of the magnetic field strength (bottom) and the inclination of the field with time at a location y=0 in the midnight meridian plane at z = 1.1 R_E above the neutral sheet (z = 0) for case C. We have assumed that the initial scale length (plasma sheet half width) is L_z = 2 R_E which accounts for some gradual thinning before onset of the unstable evolution. This location is thus well within the original plasma sheet. The magnetic field has been scaled by some unit, which can be chosen arbitrarily, to resemble the actually observed values. The different curves give the evolution at different locations in x tailward from the main X-line. The solid lines correspond to a distance of 12 R_E

representing maybe what ISEE 1 or 2 would observe within this system, the dashed lines correspond to a distance of 36 R_E closer to typical IMP 6, 7, and 8 locations, and the dotted and dash-dotted lines correspond to distances of 68 R_E and 84 R_E, respectively, not quite as far as the most distant observations by ISEE 3, but qualitatively in that direction.

Let us start with the solid and dashed curves. The inclination shows that there is only a slight southward dipping of the field starting at about the formation of the neutral line in the nearest location. At the same time the field strength starts to increase which basically shows that the plasma sheet thins and a satellite enters the lobe region. The observations in the far tail as shown by the dotted and dash-dotted curves are quite different: we can see first an enhanced northward field which can become inclined by a large angle followed by strongly southward field marking the arrival of the plasmoid. We can also see a periodicity of roughly six minutes which can be related to multiple neutral lines. At the same time the field strength within the plasmoid is reduced and highly variable. This result is very similar to the actual observations. Lui et al. (1977) pointed out that magnetic signatures on IMP at substorm expansion and plasma sheet thinning mostly consist only of a slight southward dipping. Indeed, a satellite has to be very close to the neutral sheet in this model to see strongly southward field. On the other hand, the plasmoid signatures in the far tail as seen by ISEE 3 (Hones et al., 1983) are remarkably similar to those in the computer model: the strong northward inclination followed by strong southward inclination. Even the periodicity of 5 to 10 minutes and multiple neutral line passages are a common feature.

Figure 9 shows a similar evolution at the same locations in x but at some higher distance above the neutral sheet, z = 2.4 R_E, and away from the center plane at y = 2 R_E, again for case C. For these locations we also show the azimuthal direction of the field, with = 0 corresponding to earthward field and = 180° corresponding to tailward field. Note that there are two apparent neutral sheet crossings at the most tailward location. Since the location of the "observations" and the position of the neutral sheet at z=0 are fixed in the model, this apparent crossing is caused by the dents in the field structures mentioned earlier. Otherwise the signatures are similar to those of Figure 8. Only the field does not get as strongly northward and southward.

The speed of the plasmoid can be obtained from Figures 10 and 11 for the cases C and D, respectively, by the time dependency of the location of neutral points on the x-axis. The speed in case C is about 600 km/sec for a typical Alfvén speed of 1000 km/sec close to the speed of 700 km/sec concluded by Hones et al. (1983) whereas it is somewhat lower in case). The speed in the model seems to depend on different factors which are not fully understood yet. Enhancing the lobe density and reducing the resistivity apparently leads to smaller plasmoid speed.

Let us summarize the results of this part:

1) We find a cross-tail extent of the reconnection region of about 8 to 15 R_E for the most realistic configurations, strongly dependent on the equilibrium configuration.
2) The field signatures in the near and in the distant tail are very similar in many structural details to those actually observed.

4. Energy flux and current patterns

An interesting question is that of the way the energy flows and about its conversion. Table 2 shows some typical contributions to energy inflow and outflow around the separator for case C. There are three contributions considered here, the Poynting flux $\underline{S} = \frac{1}{\mu_o} \underline{E} \times \underline{B}$, the kinetic energy flux $\frac{1}{2} v^2 \underline{v}$, and the enthalpy flux $(u+p)\,\underline{v} = \frac{5}{2} nkT\,\underline{v}$, which represents the convection of internal, or thermal energy u including deformation effects. The heat flux cannot be calculated directly in the present model because of the isothermal assumption. Typical values for each contribution are shown in Table 2 for the three spatial directions. The inflow from the z direction consists mainly of Poynting flux as is expected and the outflow in the x direction, which is much more intense is mainly convection of thermal and kinetic energy. So far, we have the typical conversion picture we are used to from two-dimensional theory. By looking at the inflow from the y direction we see that there is a significant enthalpy flux, which is more intense than the inflow from the z direction, although of course less intense than the outflow.

Another interesting feature is demonstrated by Figure 12 which shows velocity vectors in the x,z plane for case B. The center part of the figure, which is unfortunately not well to be seen because of too much overlap of the velocity arrows, represents the normal flow pattern away from the X-line or separator, marked by the circle. At the boundary of this region tailward from the separator, however, strong earthward flow occurs. This represents another inflowing energy flux mainly along the magnetic field from the tail.

The next figures shall demonstrate the typical current pattern connected with the plasmoid and the reconnection region around the separator. Figure 13 shows projections of the electric current density vectors in cross-sections of the tail at different values of x shown at the right hand side for case D.

Only the inner part with the plasma sheet is shown in each case. The look direction is tailward. The top panel is earthward from the separator, the second one close to the separator, and the two bottom ones are tailward from the separator. One can see a strong current concentration at the separator and even at some distance tailward. Earthward from the separator and even more pronounced in the distant tail the current is deviated around the center region. In the distant tail the current inside the plasmoid even changes direction causing the earlier mentioned magnetic field "dents". The same signatures can be found in the simulation with reconnection across the whole tail, case B (Fig. 14).

Another representation of these current signatures is given in Figure 15 which shows contour lines of constant cross-tail current density j_y for case B. The hatched regions correspond to currents flowing in the negative y direction opposite to the original current. The original cross-tail current forms two layers related to Petschek's (1964) slow shocks. These current layers are indeed inside the separatrix as can be seen by comparison with Figure 16 which shows magnetic field lines with the separatrix as dashed lines and the current density maxima for constant x connected by dotted lines. The current layers coincide with the flow vorticity layers where the plasma flow direction changes from tailward to earthward, shown in Figure 12.

Typical current deviations in the equatorial x,y plane and several other parallel planes are demonstrated by Figure 17 for case C. These deviations produce earthward currents on the dawn side and tailward currents on the dusk side earthward from the neutral line (dashed line). The same current deviation is also found in the case with reconnection across the whole tail (Figure 18). This current deviation does not directly lead to field-aligned currents in the same direction, because there is a rotation of the magnetic field direction in

the same direction as the current deviation (Figure 19). A field-aligned current system that is actually found in case B is shown in Figure 20 by contour lines of constant parallel current density in a cross-section of the tail at x=-8 earthward from the separator. Earthward currents are indicated by single hatching tailward currents by cross-hatching. The main field-aligned current system in this cross-section has the signatures of so-called region 2 currents (Iijima and Potemra, 1976) as found near the earth, earthward on the duskside and tailward on the dawnside. They are surrounded by some oppositely directed currents corresponding to the region 1 currents observed close to the earth. These currents, however, are smaller in magnitude and are not found in all our simulations.

Figure 21, taken from Hones et al. (1982), demonstrates how the main field-aligned current system is produced in our model. The figure shows magnetic field lines on the duskside of the tail above the neutral sheet as seen from the tail in the direction of the earth. Thin lines show the projections of the field lines into the equatorial plane z=0. We see that at the X-line the lowest field line closest to the neutral sheet is convected the most toward the midnight meridian plane y=0, whereas higher field lines are less affected by this convection. The inward convection along the X-line from the flanks of the tail therefore produces a shear of the magnetic field and it is this shear that is responsible for the field-aligned currents with the "region 2" signatures.

5. Conclusions

We have demonstrated the usefulness of MHD simulations in a realistic three-dimensional magnetotail geometry. Energization of the plasma due to conversion of magnetic into kinetic energy is found without any external driving force. The computer simulations have produced many additional features

which can be found in satellite observations in the magnetotail, most recently by using the ISEE 3 satellite at distances up to 220 R_E. Among those features are the spatial limitation of reconnection in the cross-tail y direction, a finite scale of the plasmoid structure in the x direction along the tail usually connected with the appearance of multiple neutral lines, and filamentary structures of the cross-tail current in the z direction caused by characteristic current deviations through the edges of the plasmoid. A characteristic difference of magnetotail field signatures in the distant tail with those in the nearer tail as found in the model showed a remarkable resemblance of actual observations.

The current system of the plasmoid and at the reconnection site were discussed and it was demonstrated that velocity shear arising in the three-dimensional reconnection model produced field-aligned currents with the signatures of the observed "region 2" currents. The full observed field-aligned current system, however, was not obtained, most likely because the boundary conditions of the model did not include a realistic interaction of the magnetotail with the solar wind and with the ionosphere.

Acknowledgment. This work was performed under the auspices of the U.S. Department of Energy.

References

Birn, J., The resistive tearing mode by a two-dimensional finite difference method, in "Computing in Plasma Physics and Astrophysics", edited by D. Biskamp, P. 4, Garching, W. Germany, 1976.

Birn, J., Self consistent magnetotail theory: General solution for the quiet tail with vanishing field-aligned currents, J. Geophys. Res., 84, 5143, 1979.

Birn, J., and E. W. Hones, Jr., Three-dimensional computer modeling of dynamic reconnection in the geomagnetic tail, J. Geophys. Res., 86, 6802, 1981.

Hones, E. W., Jr., J. Birn, S. J. Bame, G. Paschmann, and C. T. Russell, On the three-dimensional magnetic structure of the plasmoid created in the magnetotail at substorm onset, Geophys. Res. Lett., 9, 203, 1982.

Hones, E. W., Jr., D. N. Baker, S. J. Bame, W. C. Feldman, J. T. Gosling, D. J. McComas, R. D. Zwickl, J. Slavin, E. J. Smith, and B. T. Tsurutani, Structure of the magnetotail at 220 R_E and its response to geomagnetic activity, submitted to Geophys. Res. Lett., 1983.

Lui, A.T.Y., C. -I. Meng, and S. -I. Akasofu, Search for the magnetic neutral line in the near-earth plasma sheet, 2, systematic study of IMP 6 magnetic field observations, J. Geophys. Res., 82, 1547, 1977.

Parker, E. N., The solar flare phenomenon and the theory of reconnection and annihilation of magnetic fields, Astrophys. J. Suppl. Series, 8, 177, 1963.

Petschek, H. E., Magnetic field annihilation, in "The Physics of Solar Flares", edited by W. N. Hess, NASA SP-50, p. 425, Washington D.C., 1964.

Sato, T., and T. Hayashi, Externally driven magnetic reconnection and a powerful magnetic energy converter, Phys. Fluids, 22, 1189, 1979.

Sweet, P. A., The neutral point theory of solar flares, in "Electromagnetic Phenomena in Cosmic Physics", edited by B. Lehnert, p. 123, Cambridge Univ. Press, 1958.

Table 1. Parameters of the different computer runs

Run	Plasma sheet broadening	Lobe density n_L	Magnetic Reynolds number S
A	2	0.25	200
B	1	0.1	200
C	2	0.05	200
D	2	0.25	1000

Table 2. Energy inflow and outflow around the separator (X-line) for case C.

	Inflow from z (erg/cm^2 sec)	Inflow from y	Outflow in x earthward (erg/cm^2 sec)	Outflow in x tailward
Poynting flux	.021	.018	.003	.001
Bulk kinetic energy flux	.002	.008	.147	.431
Enthalpy flux	.006	.090	.451	.480

Fig. 1 Schematic representation of a quarter tail section used as initial configuration. Solid lines with arrows represent magnetic field lines in the midnight meridian plane z=0 and on some surface close to the magnetopause. The hatched region indicates the plasma sheet.

Fig. 2 Magnetic field lines in the x,z plane for run A (see text). After Birn and Hones (1981).

Fig. 3 Flow vectors and magnetic neutral lines (dotted lines) in the x,y plane for run A. After Birn and Hones (1981).

Fig. 4 Flow vectors and magnetic neutral lines (dotted lines) in the x,y plane for run B.

Fig. 5 Magnetic field lines in the x,z plane for run B.

Fig. 6 Magnetic field lines in the x,z plane for run C.

Fig. 7 Magnetic field lines in the x,z plane for run D.

Fig. 8 Evolution of the magnetic field strength (bottom part) and latitude for run C at different locations indicated in the figure.

Fig. 9 Evolution of the magnetic field latitude , longitude , and magnitude B for run C at different locations indicated in the figure.

Fig. 10 Location of neutral points on the x axis as a function of time for case C. Solid lines depict X point locations and dashed lines depict O point locations (normalized units).

Fig. 11 Location of neutral points on the x axis as a function of time for case D similar to Figure 10.

Fig. 12 Velocity vectors in the x,z plane at t = 200 (normalized units) for case B.

Fig. 13 Projections of electric current density vectors for case D in different cross-sections of the tail as indicated by the locations in x tailward from the near-earth boundary (normalized units).

Fig. 14 Projections of electric current density vectors for case B in a similar representation as in Figure 13.

Fig. 15 Contour lines of constant cross-tail current density j_y in the x,z plane for case B. The hatched regions correspond to currents flowing in the negative y direction with $j_y < -0.2$ (normalized units).

Fig. 16 Magnetic fieldlines in the x,z plane at t = 200 for case B. The dashed line represents the separatrix and the dotted line represents the current density maxima for constant x.

Fig. 17 Projections of electric current density vectors in the x,y plane and several other planes as indicated on the right side for case C.

Fig. 18 Projections of electric current density vectors for case B in the same representation as in Figure 17.

Fig. 19 Projections of magnetic field vectors in planes z = const as indicated in the figure, for case B.

Fig. 20 Contours of constant field-aligned current density in the cross-section x = -8 at t = 200 (normalized units) for case B. Single hatching indicates earthward ~~flow~~ field-aligned currents and cross-hatching indicates tailward ~~flow~~. field-aligned currents

Fig. 21 Three-dimensional representation of magnetic fieldlines after Hones et al. (1982). Projections of the magnetic fieldlines into the x,y plane are shown by ~~e~~light lines.

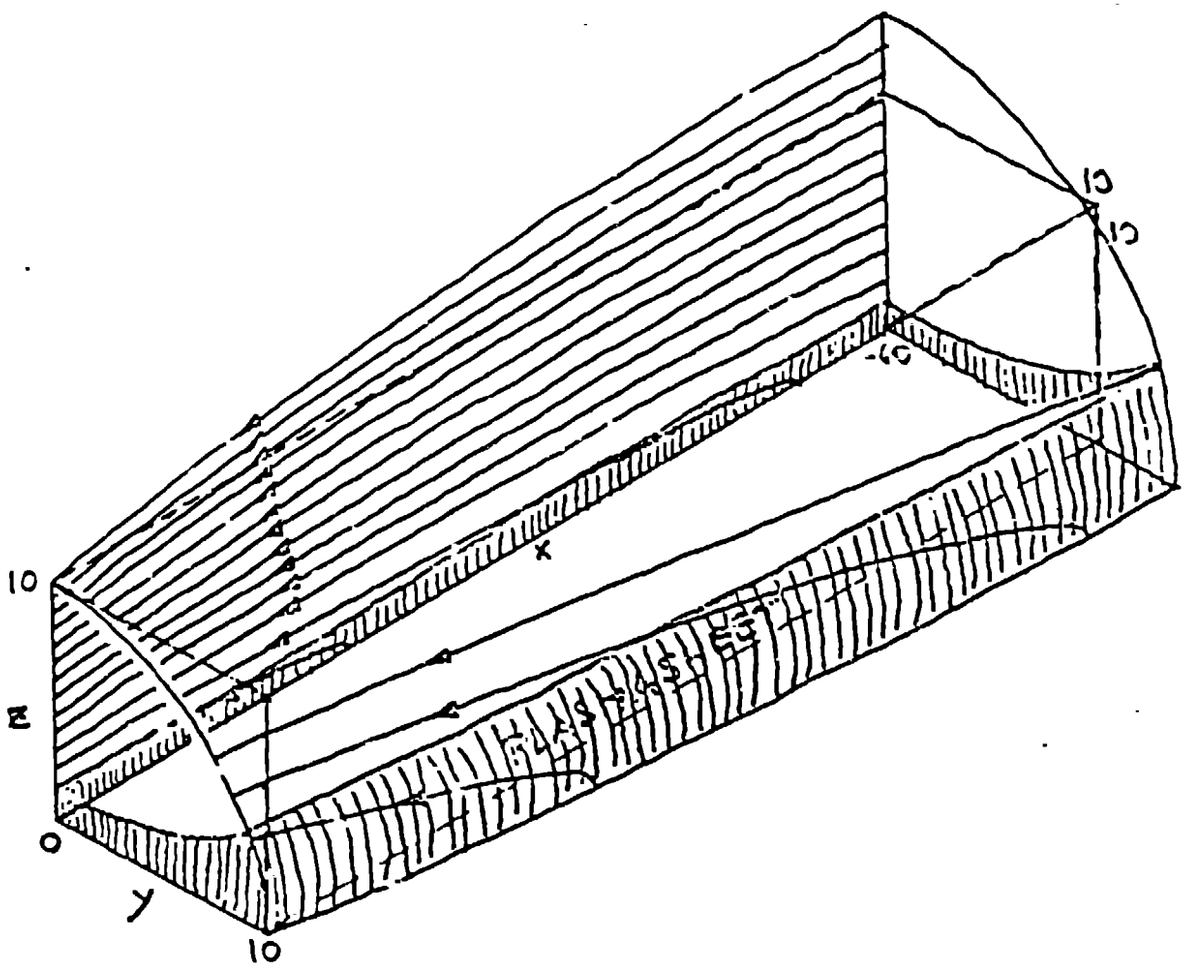
10
z
0
y
10
x
10
10

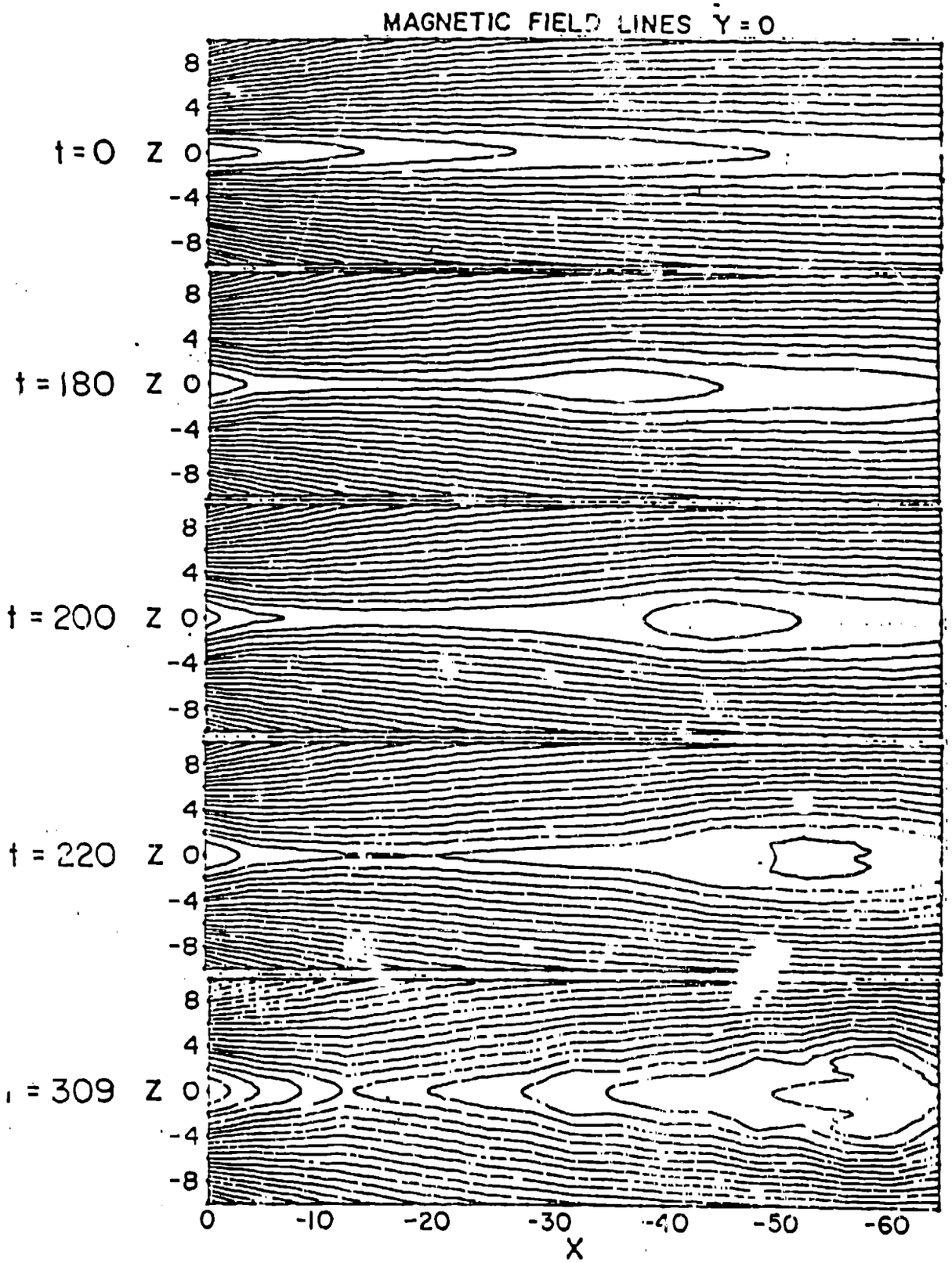
MAGNETIC FIELD LINES Y = 0
t = 0
t = 180
t = 200
t = 220
t = 309
Z
8
4
0
-4
-8
0
-10
-20
-30
-40
-50
-60
X

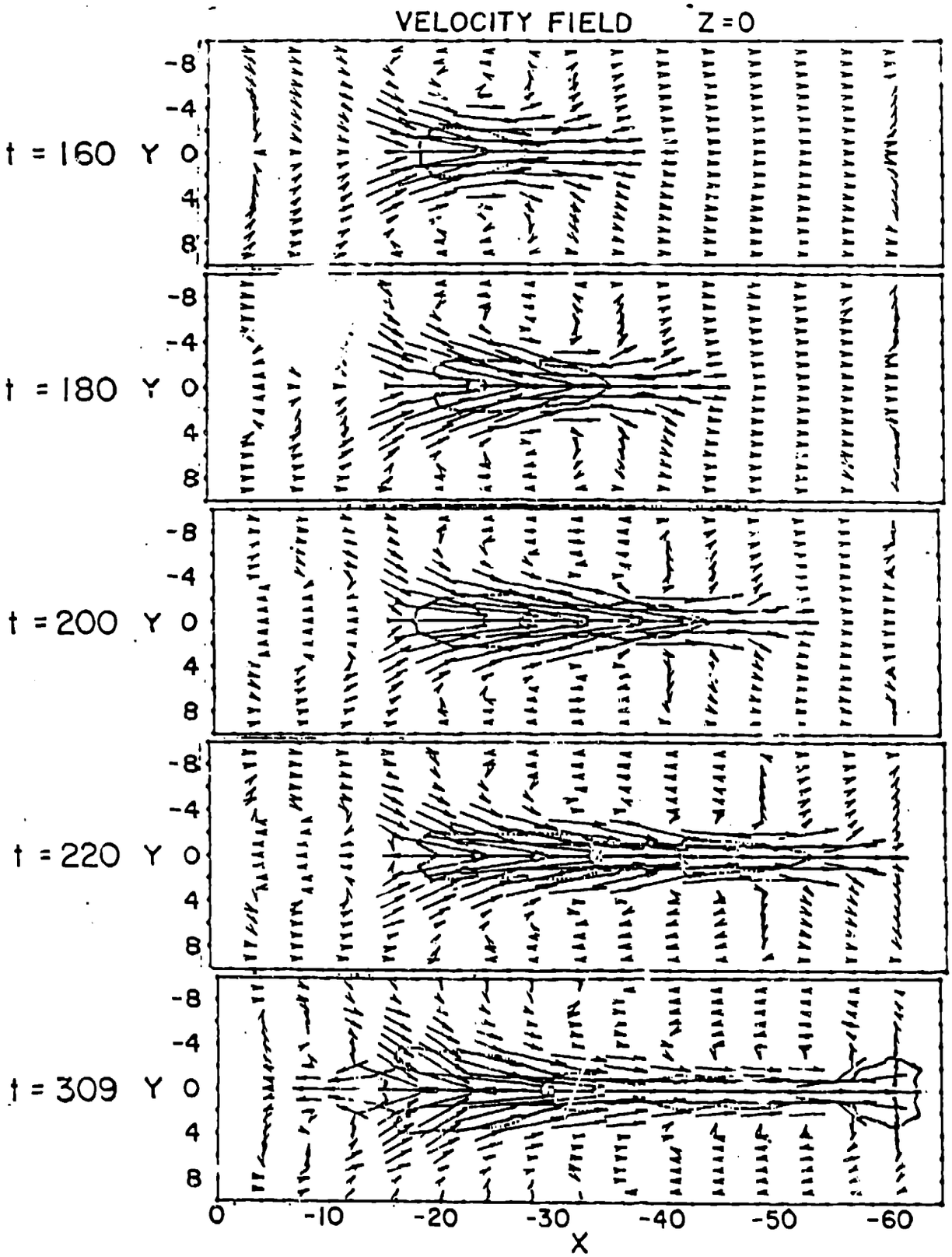
VELOCITY FIELD Z=0
t = 160 Y
t = 180 Y
t = 200 Y
t = 220 Y
t = 309 Y
-8
-4
0
4
8
0
-10
-20
-30
-40
-50
-60
X

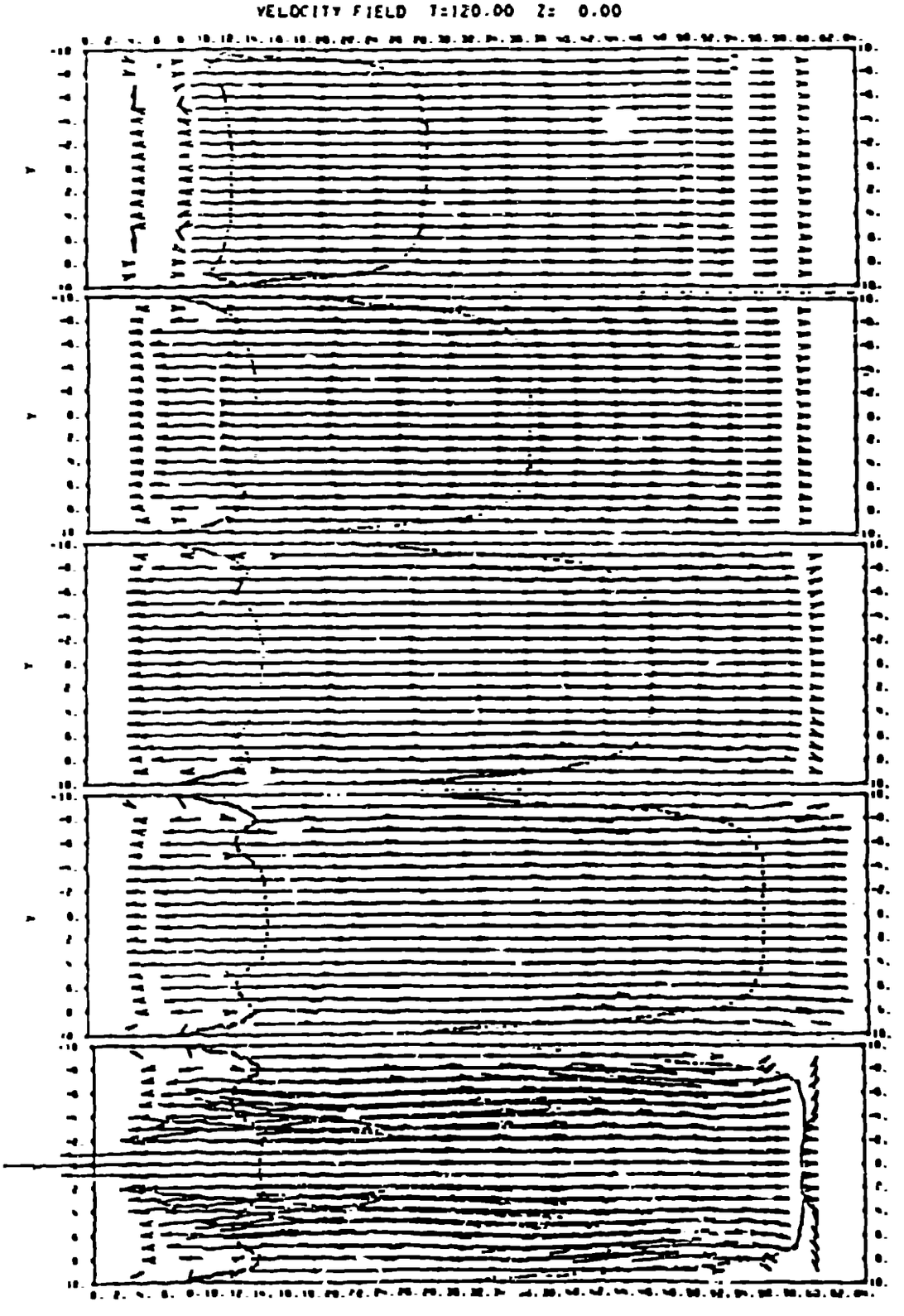
VELOCITY FIELD T=120.00 Z= 0.00
t = 120
140
160
180
200
X

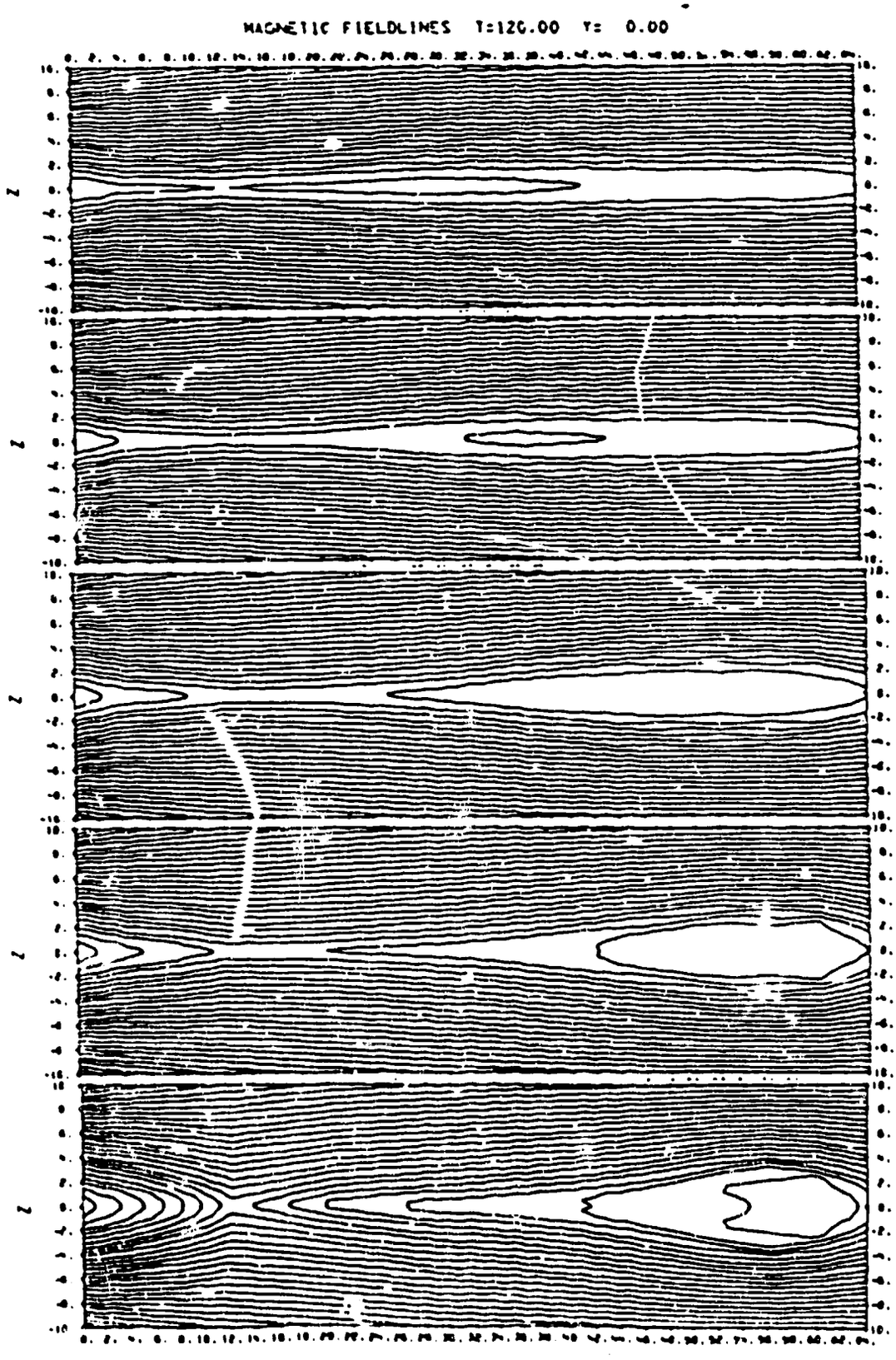
MAGNETIC FIELDLINES T=120.00 Y= 0.00
Z
X
t=120
140
160
180
200

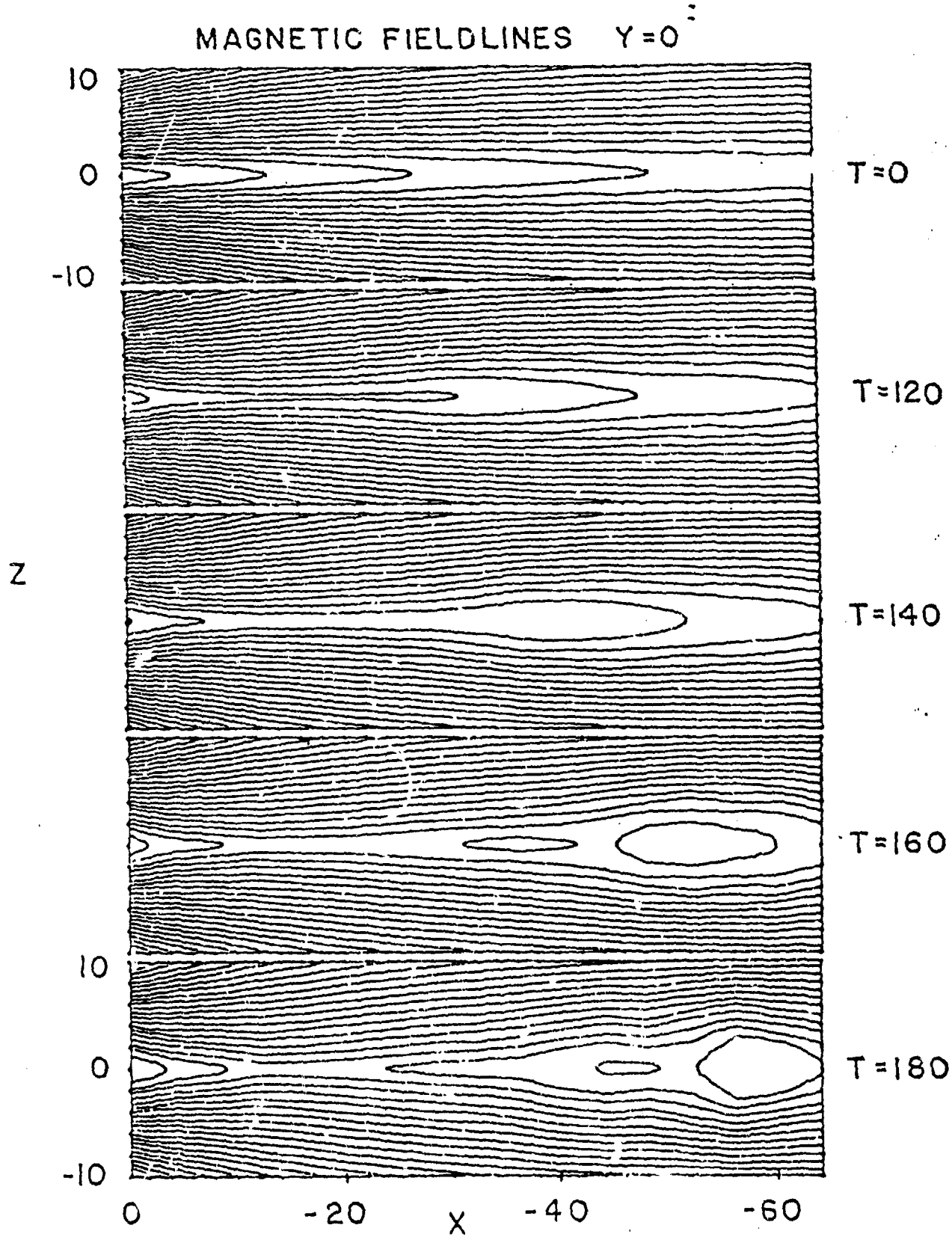
MAGNETIC FIELDLINES Y=0
10
0
-10
T=0
T=120
T=140
T=160
T=180
Z
10
0
-10
0
-20
X
-40
-60

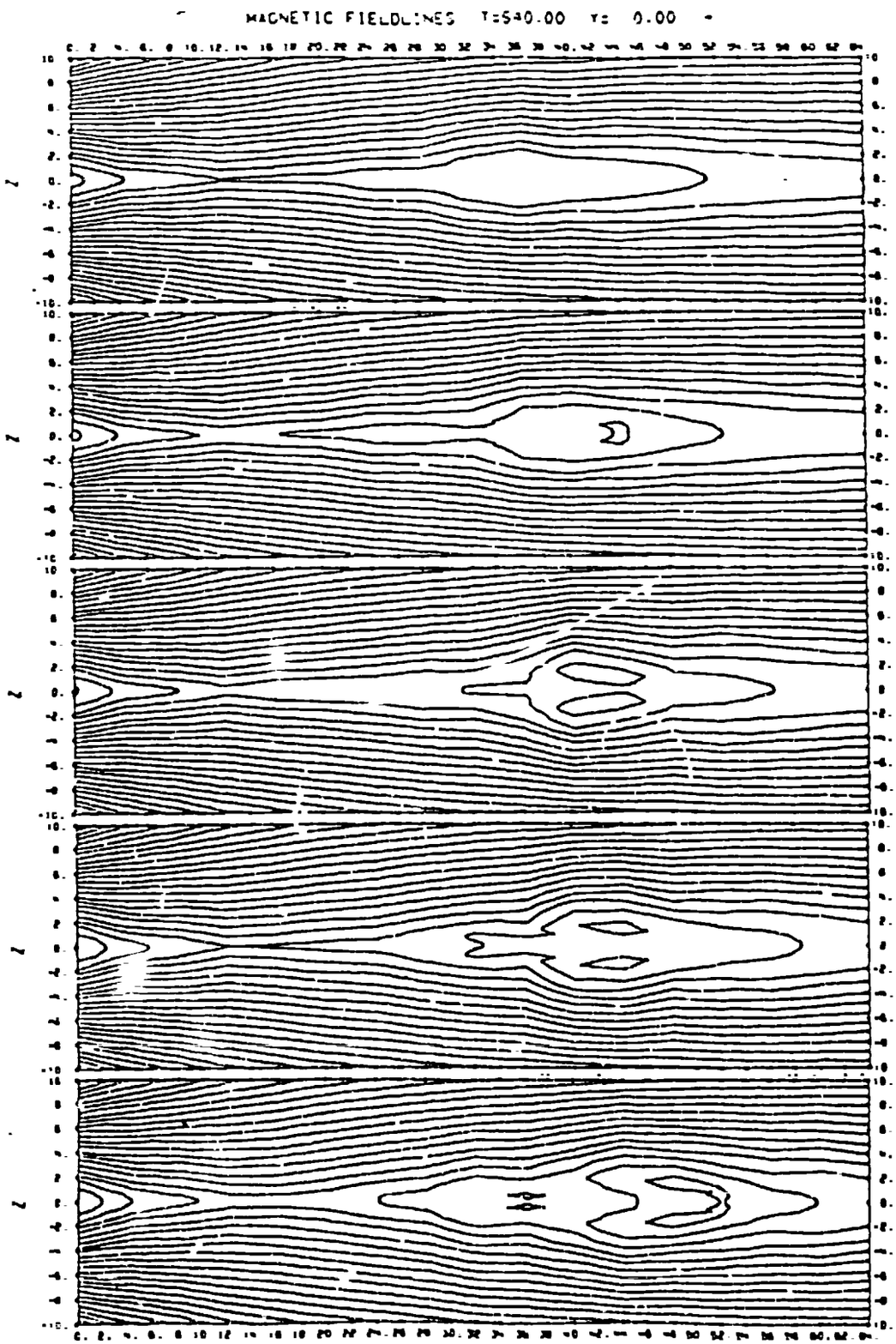
MAGNETIC FIELDLINES T=540.00 Y= 0.00
t=540
550
560
570
580
Z
X

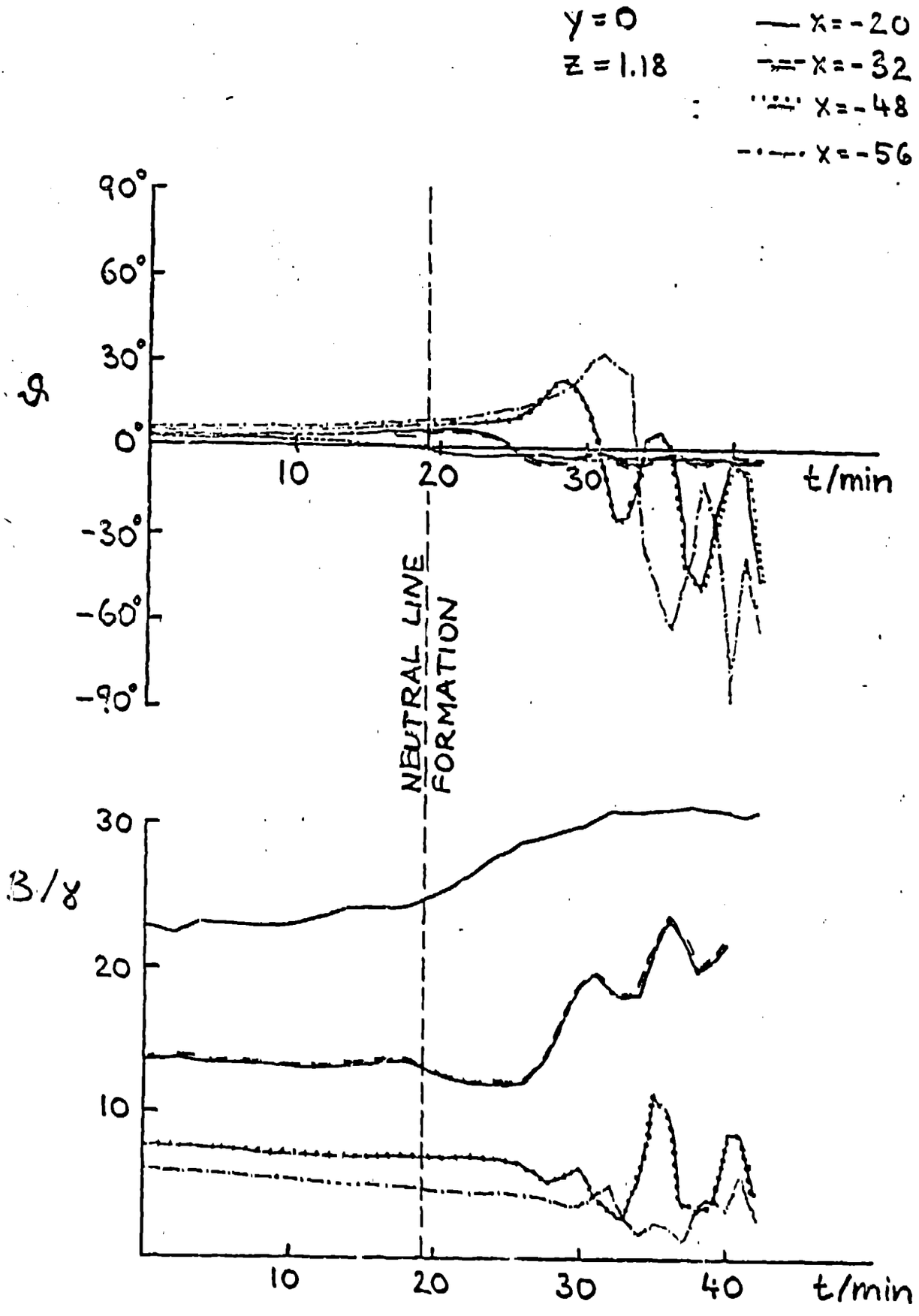
y = 0
z = 1.18
x = -20
x = -32
x = -48
x = -56
90°
60°
30°
0°
-30°
-60°
-90°
ϑ
10
20
30
t/min
NEUTRAL LINE FORMATION
30
20
10
B/α
10
20
30
40
t/min

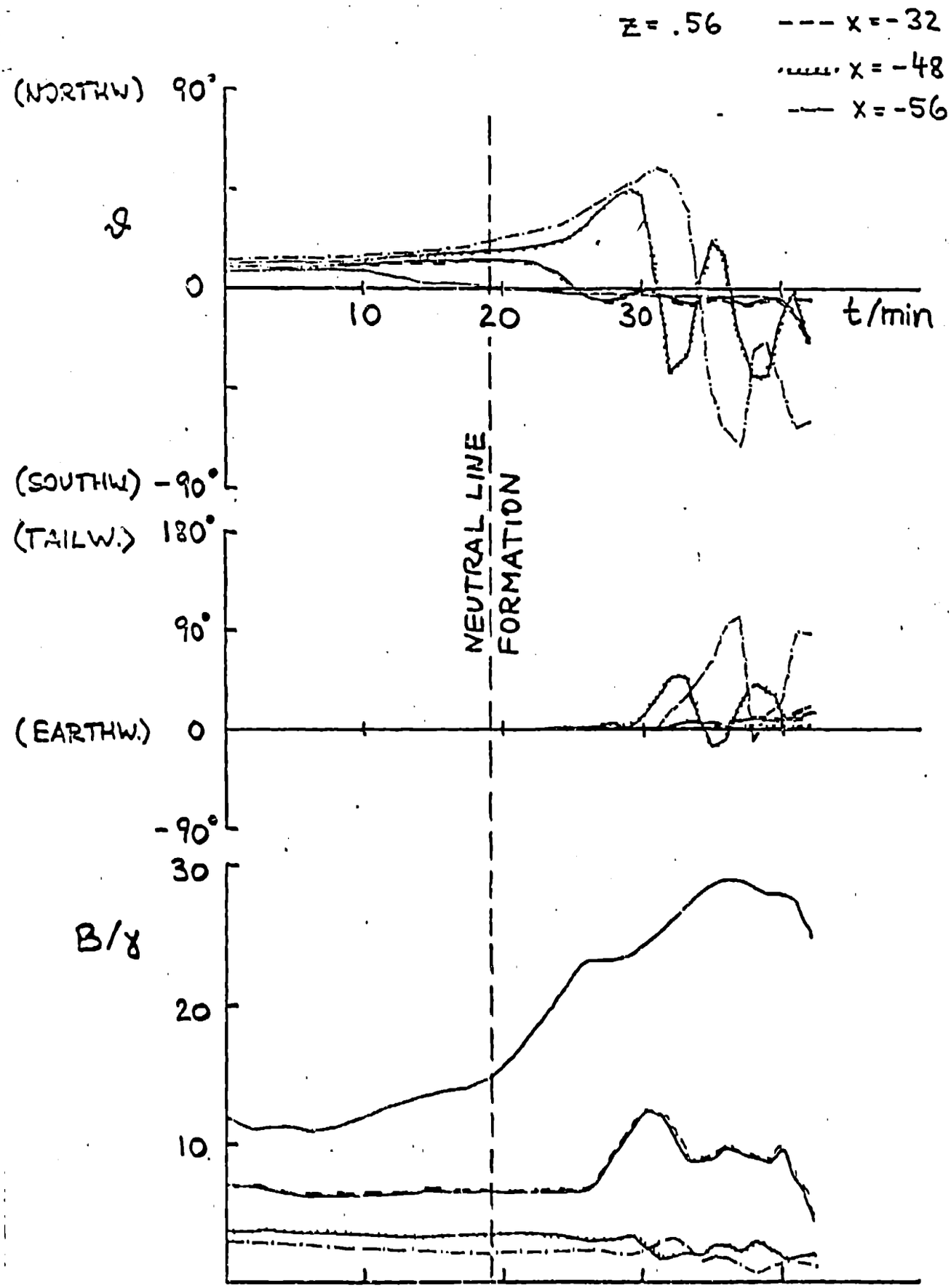
z = .56
--- x = -32 "IMP 8"
x = -48 "ISEE 3"
—— x = -56
(NORTHW) 90°
ϑ
0
10
20
30
t/min
(SOUTHW) -90°
(TAILW.) 180°
90°
NEUTRAL LINE FORMATION
(EARTHW.) 0
-90°
30
B/γ
20
10

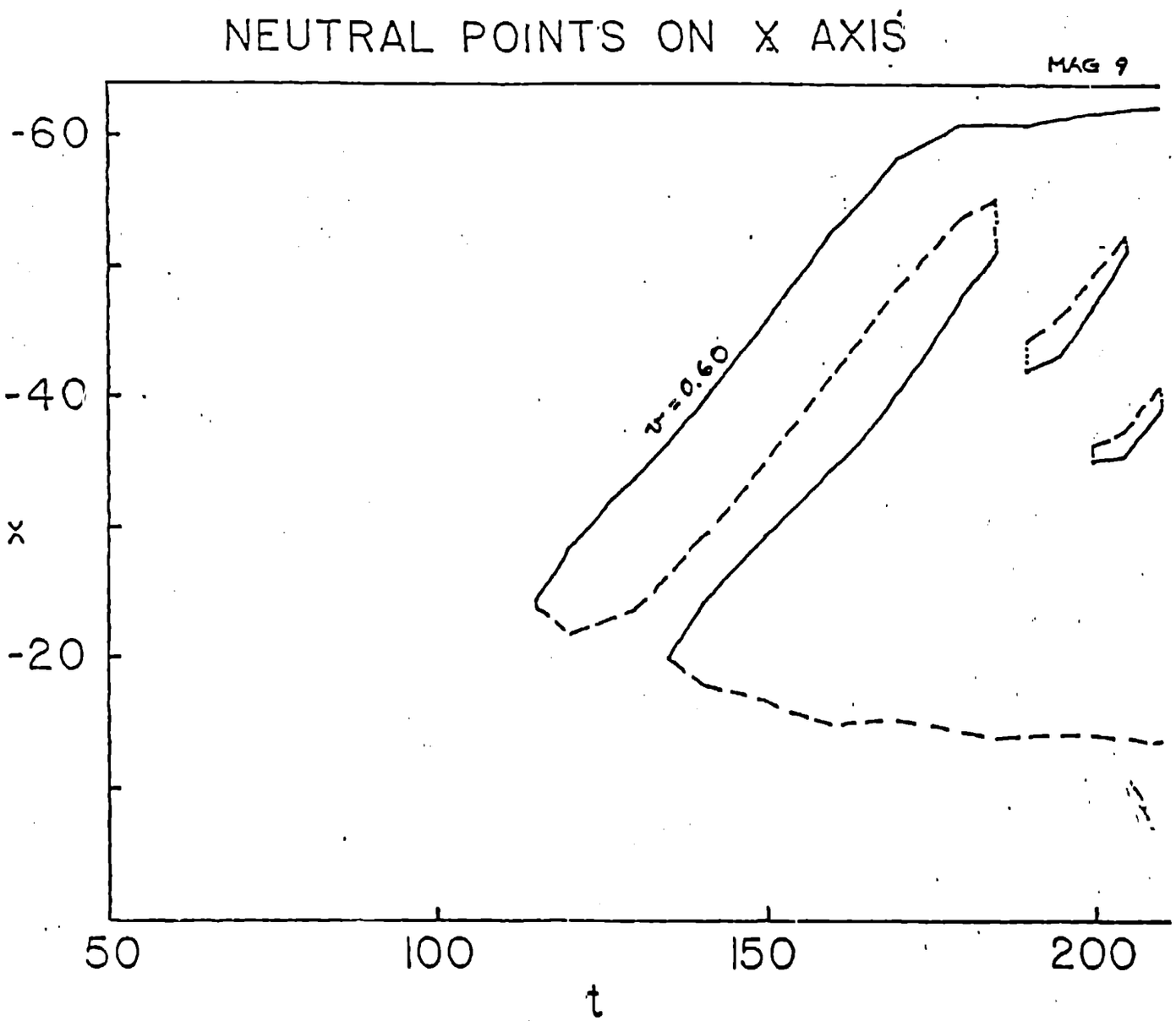
NEUTRAL POINTS ON X AXIS
MAG 9
-60
-40
-20
x
v=0.60
50
100
150
200
t

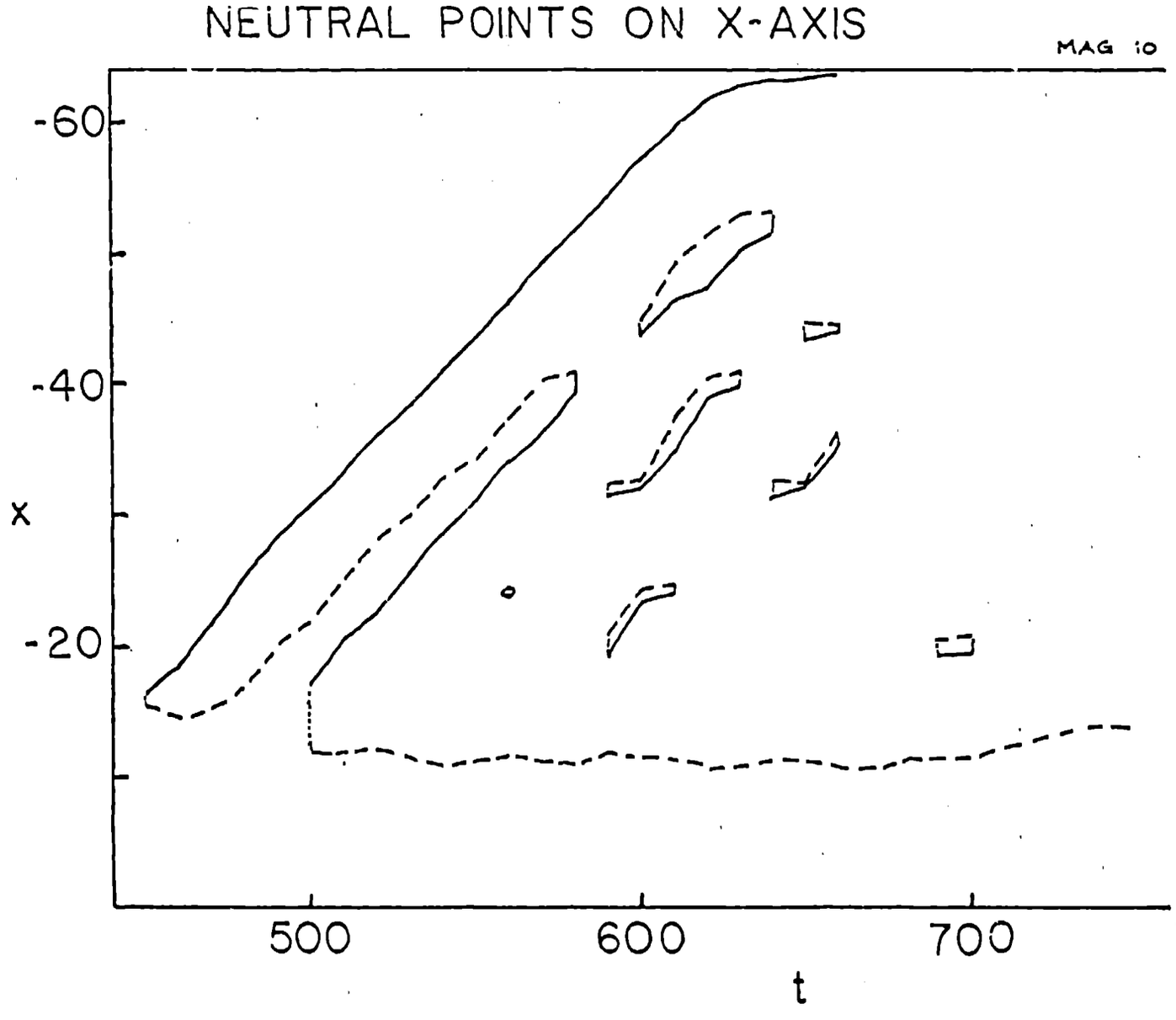
NEUTRAL POINTS ON X-AXIS
MAG 10
-60
-40
-20
x
500
600
700
t

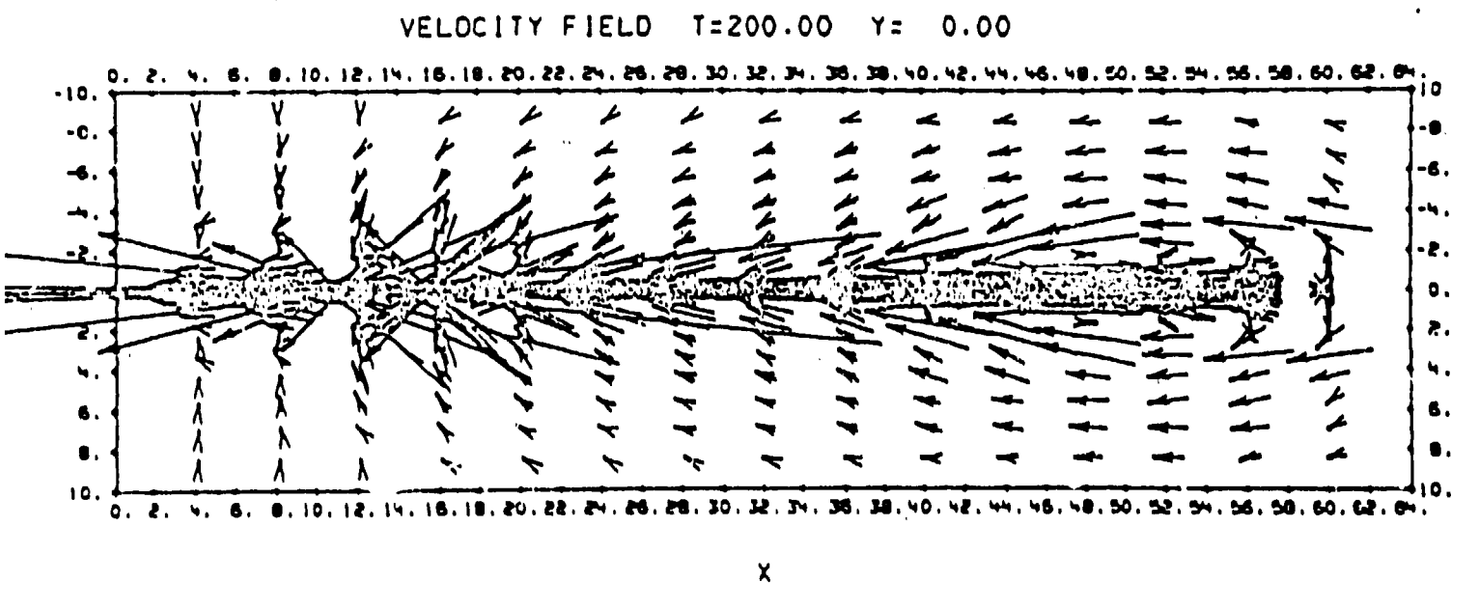
VELOCITY FIELD T=200.00 Y= 0.00
X

ELECTRIC CURRENT DENSITY
t=750
2
-2
2
Z
-2
2
-2
2
-2
-10
0
10
Y
X = -1
1
2
4

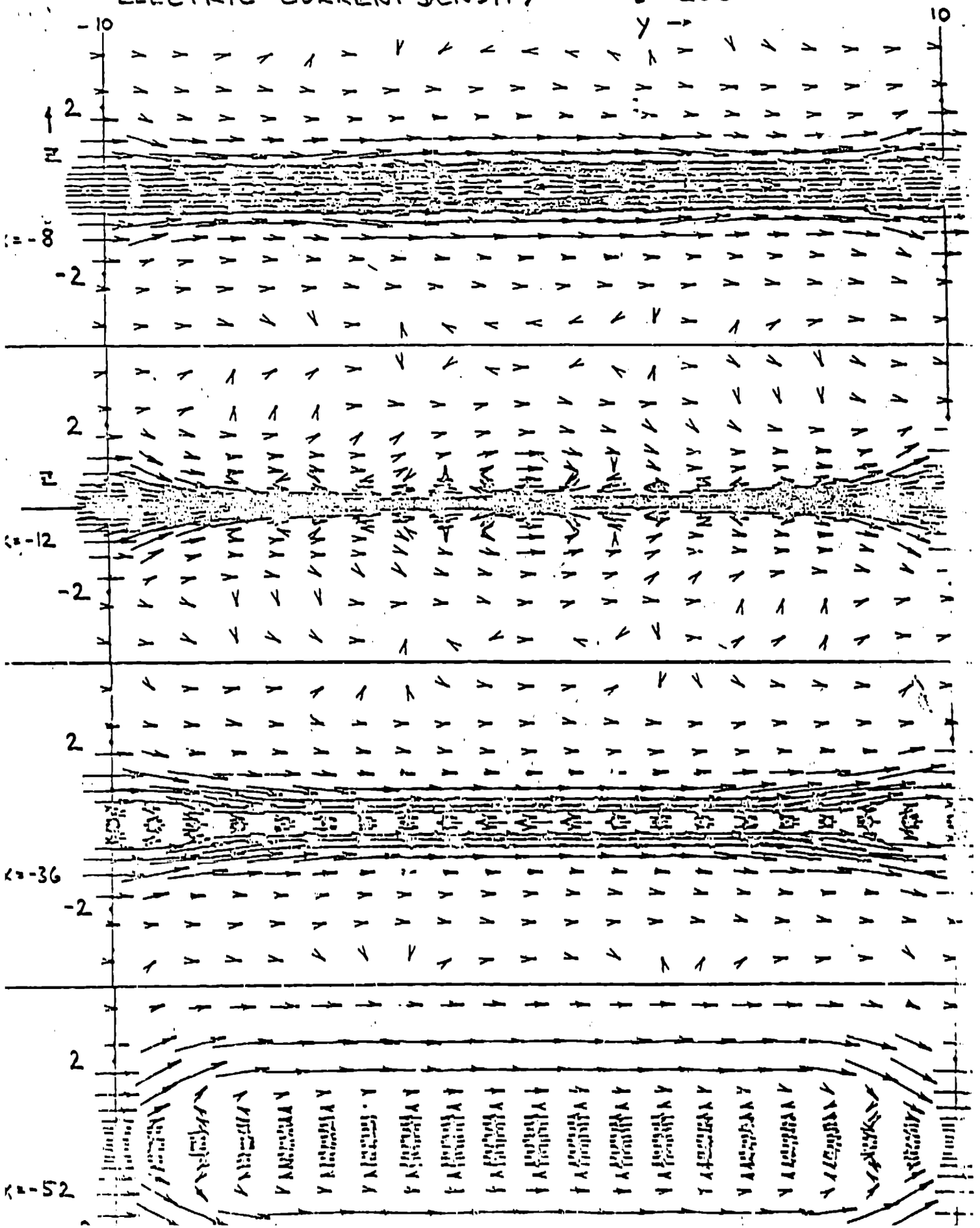
ELECTRIC CURRENT DENSITY
t = 200
y →
-10
10
2
-2
z
x=-8
2
-2
z
x=-12
2
x=-36
-2
2
x=-52

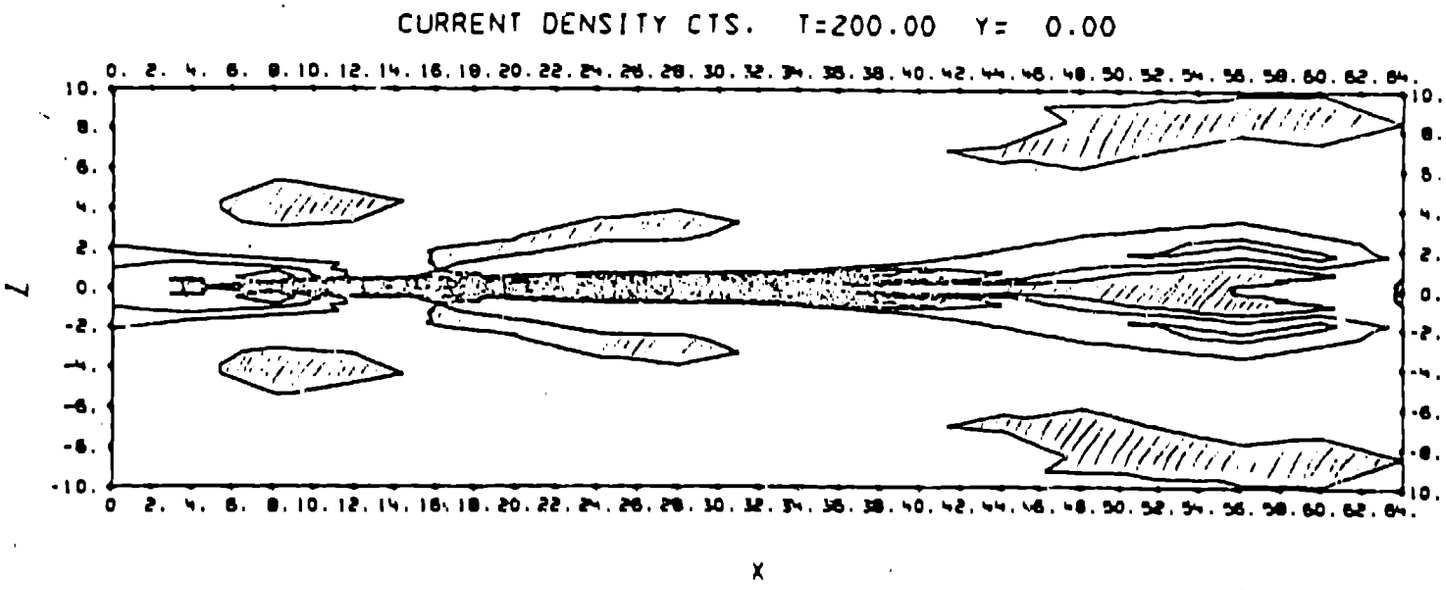
CURRENT DENSITY CTS. T=200.00 Y= 0.00
0. 2. 4. 6. 8. 10. 12. 14. 16. 18. 20. 22. 24. 26. 28. 30. 32. 34. 36. 38. 40. 42. 44. 46. 48. 50. 52. 54. 56. 58. 60. 62. 64.
10. 8. 6. 4. 2. 0. -2. -4. -6. -8. -10.
Z
X

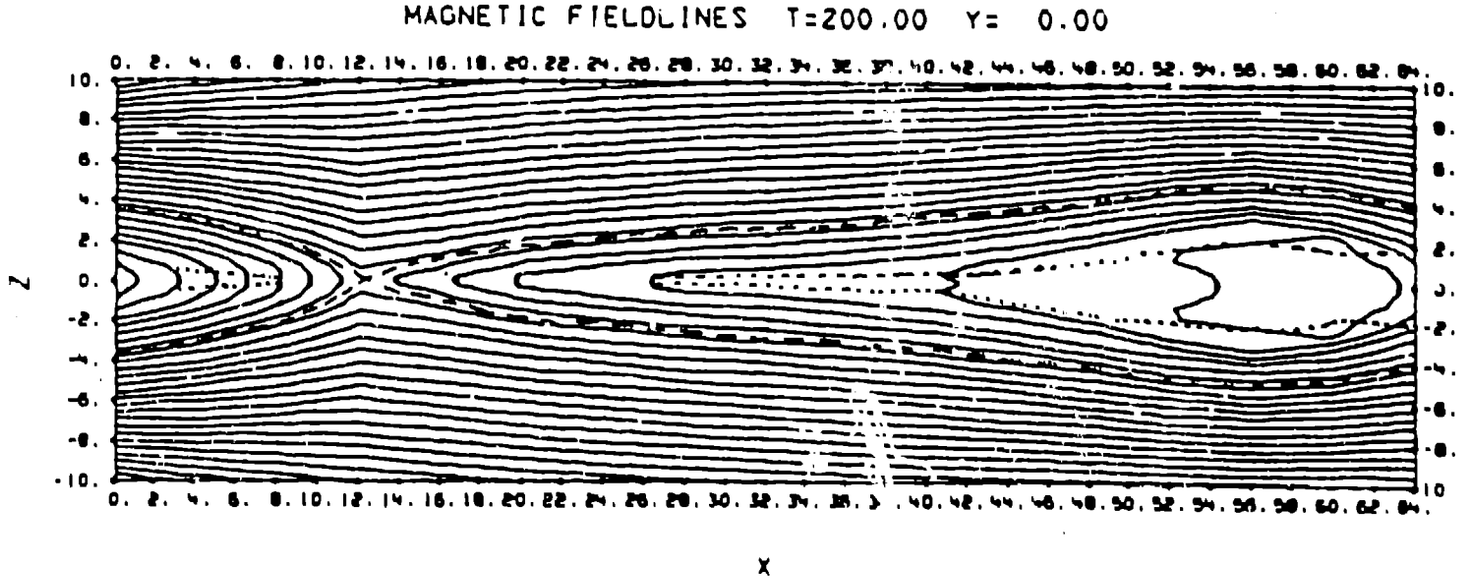
MAGNETIC FIELDLINES T=200.00 Y= 0.00
Z
X

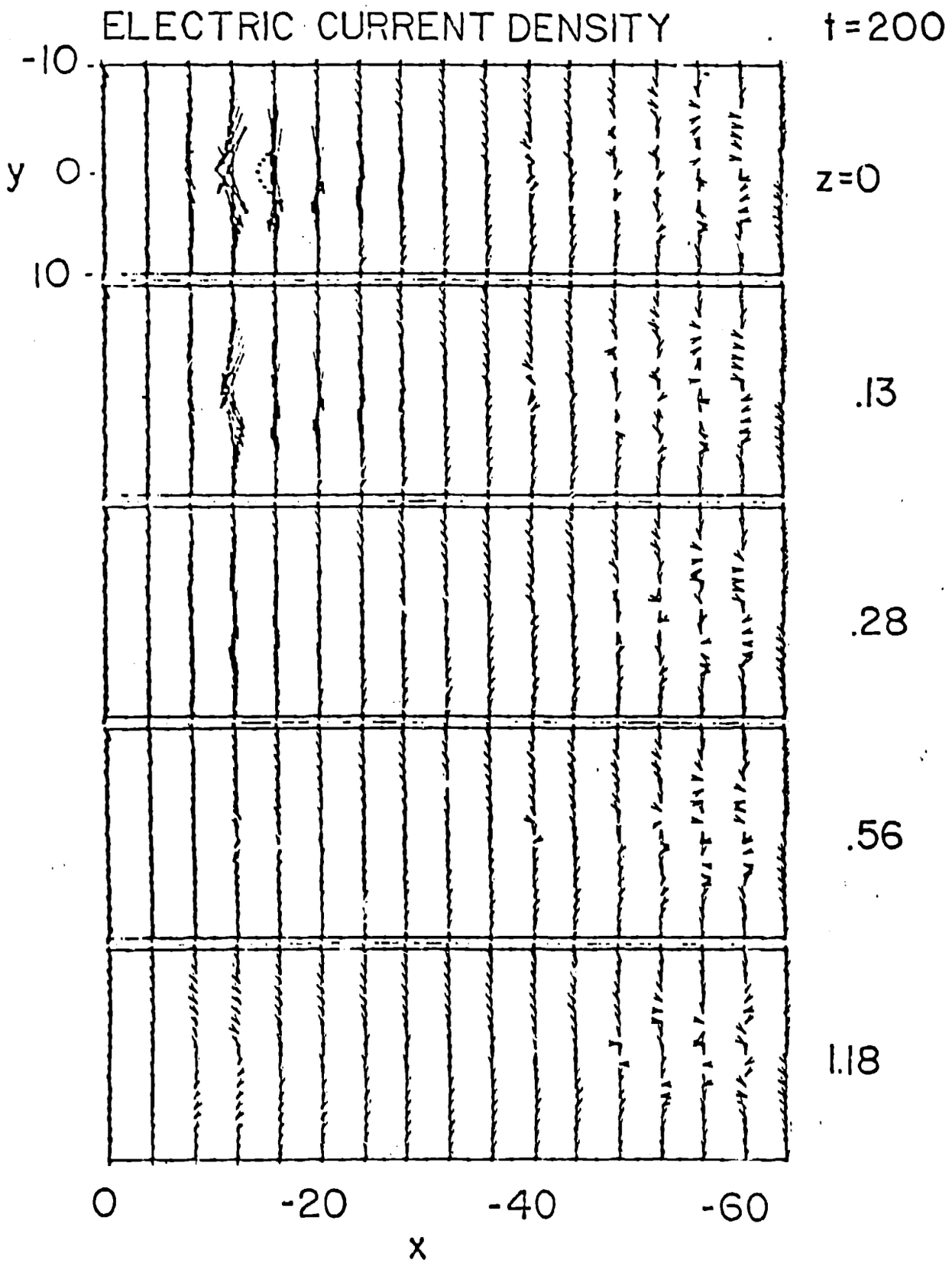
ELECTRIC CURRENT DENSITY
t=200
-10
y 0
10
z=0
.13
.28
.56
1.18
0
-20
-40
-60
x

Fig. 17

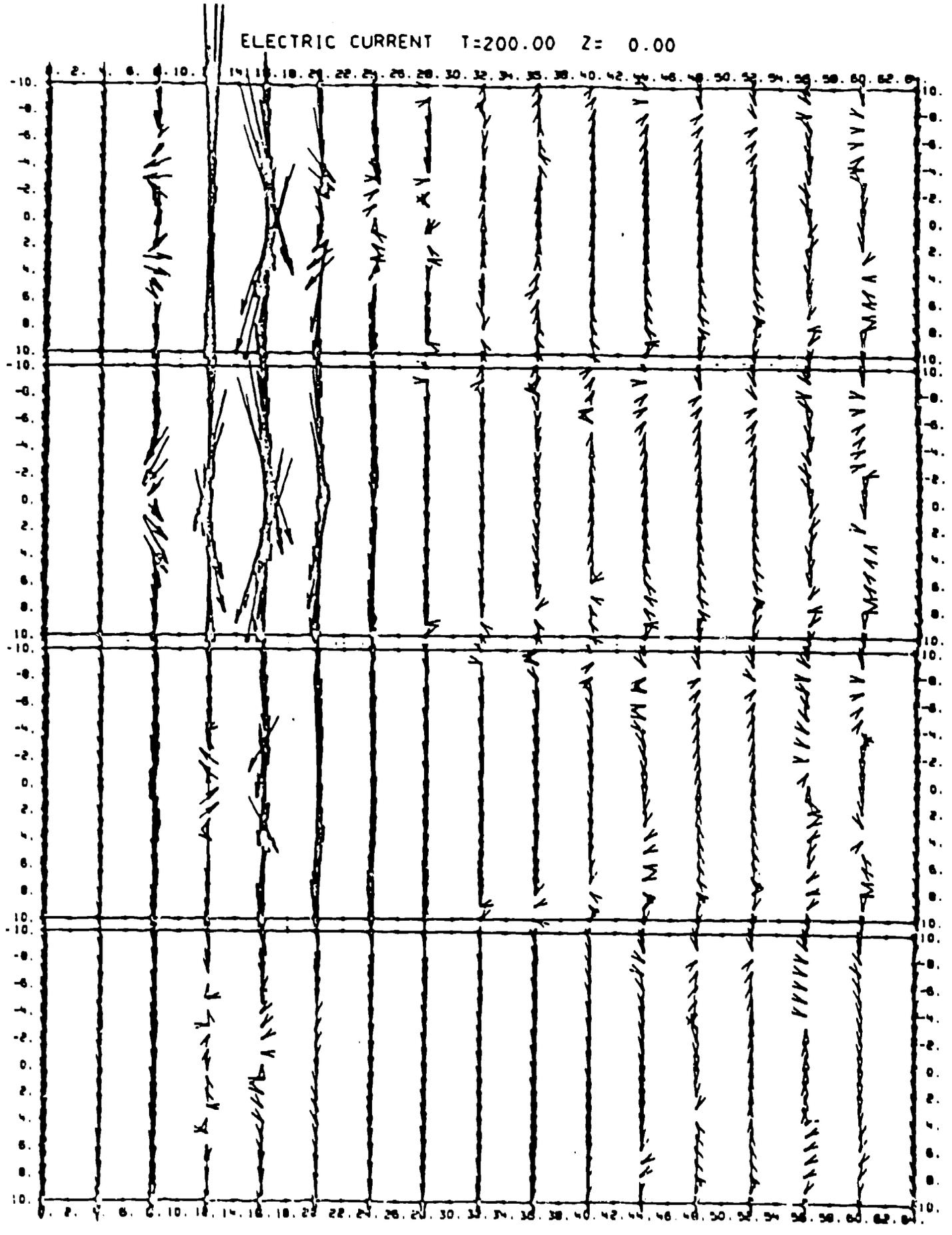
ELECTRIC CURRENT T=200.00 Z= 0.00

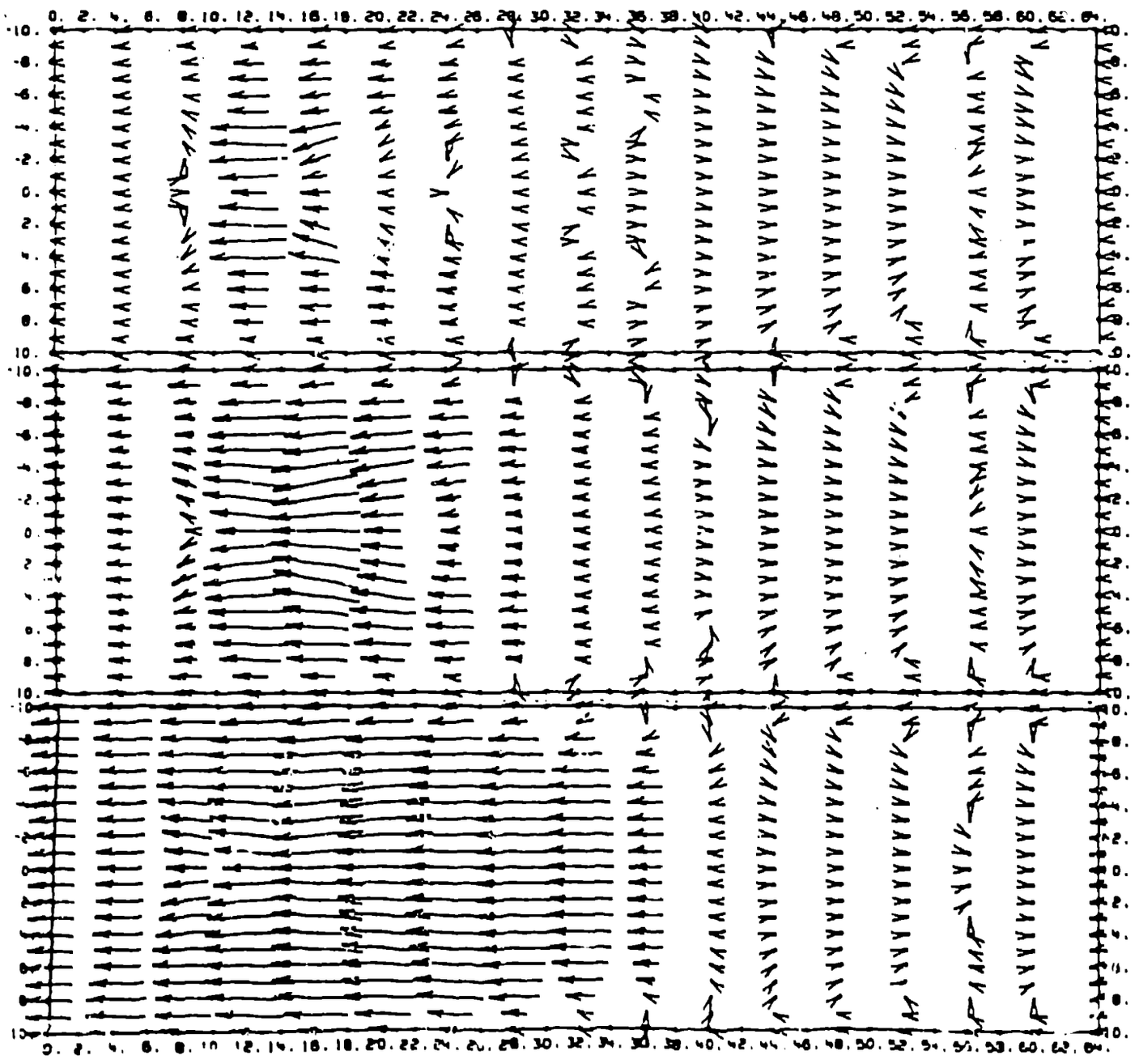
MAGNETIC FIELD T=200.00 Z= .13
Y
X

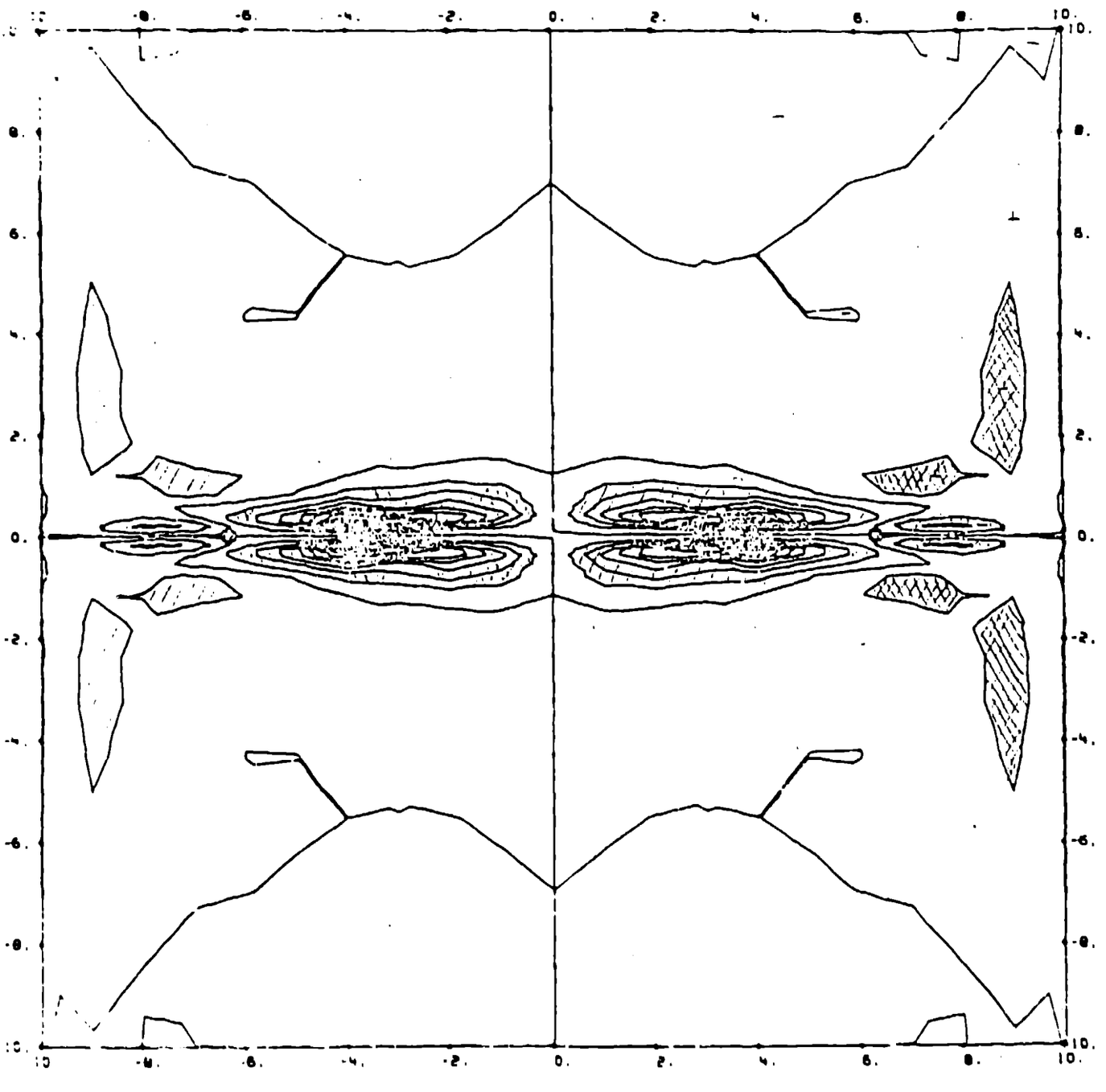
J-PARALLEL CONTOURS T=200.00 X= -8.000
-10.
-8.
-6.
-4.
-2.
0.
2.
4.
6.
8.
10.
Z
Y

THEORETICAL 3-D MAGNETIC CONFIGURATION
(T=180)